

## Arctic Sea Ice Loss, Long-Term Trends in Extratropical Wave Forcing, and the Observed Strengthening of the QBO-MJO Connection

Lon L. Hood<sup>1</sup>  and Charles A. Hoopes<sup>1,2</sup> 

<sup>1</sup>Lunar and Planetary Laboratory, University of Arizona, Tucson, AZ, USA, <sup>2</sup>Department of Hydrology & Atmospheric Sciences, University of Arizona, Tucson, AZ, USA

**Key Points:**

- A stronger modulation of the Madden-Julian oscillation by the stratospheric quasi-biennial oscillation has existed since the early 1980s
- Tropical stratospheric static stability has declined since the late 1970s due partly to increases in early winter extratropical wave forcing
- Larger sea level pressure anomalies over northern Eurasia due to Arctic sea ice loss are a possible cause of the increasing wave forcing

**Supporting Information:**

Supporting Information may be found in the online version of this article.

**Correspondence to:**

L. L. Hood,  
lon@lpl.arizona.edu

**Citation:**

Hood, L. L., & Hoopes, C. A. (2023). Arctic Sea ice loss, long-term trends in extratropical wave forcing, and the observed strengthening of the QBO-MJO connection. *Journal of Geophysical Research: Atmospheres*, 128, e2023JD039501. <https://doi.org/10.1029/2023JD039501>

Received 19 JUN 2023  
Accepted 25 NOV 2023

**Author Contributions:**

**Conceptualization:** Lon L. Hood  
**Formal analysis:** Lon L. Hood, Charles A. Hoopes  
**Funding acquisition:** Lon L. Hood  
**Investigation:** Lon L. Hood, Charles A. Hoopes  
**Methodology:** Lon L. Hood, Charles A. Hoopes  
**Project Administration:** Lon L. Hood  
**Resources:** Lon L. Hood  
**Software:** Lon L. Hood, Charles A. Hoopes  
**Supervision:** Lon L. Hood  
**Validation:** Lon L. Hood  
**Writing – original draft:** Lon L. Hood  
**Writing – review & editing:** Charles A. Hoopes

**Abstract** A modulation has been identified of the tropical Madden-Julian oscillation (MJO) by the stratospheric quasi-biennial oscillation (QBO) such that the MJO in boreal winter is ~40% stronger and persists ~10 days longer during the easterly QBO phase (QBOE) than during the westerly phase. A proposed mechanism is reductions of tropical lower stratospheric static stability during QBOE caused by (a) the QBO induced meridional circulation; and (b) QBO influences on extratropical wave forcing of the stratospheric residual meridional circulation during early winter. Here, long-term variability of the QBO-MJO connection and associated variability of near-tropopause tropical static stability and extratropical wave forcing are investigated using European Center reanalysis data for the 1959–2021 period. During the most reliable (post-satellite) part of the record beginning in 1979, a strengthening of the QBO-MJO modulation has occurred during a time when tropical static stability in the lowermost stratosphere and uppermost troposphere has been decreasing and extratropical wave forcing in early winter has been increasing. A high inverse correlation ( $R = -0.87$ ) is obtained during this period between early winter wave forcing anomalies and wintertime tropical lower stratospheric static stability. Regression relationships are used to show that positive trends in early winter wave forcing during this period have likely contributed to decreases in tropical static stability, favoring a stronger QBO-MJO connection. As shown in previous work, increased sea level pressure anomalies over northern Eurasia produced by Arctic sea ice loss may have been a significant source of the observed positive trends in early winter wave forcing.

**Plain Language Summary** The tropical Madden-Julian oscillation, also called the 40–50-day oscillation, is a propagating pattern of tropical convection and precipitation that is a major driver of intraseasonal climate variability. Recent studies have found that (a) it is modulated by stratospheric forcings like the quasi-biennial oscillation (QBO); and (b) the QBO modulation appears to have been strengthening since the early 1980s. A possible cause of the QBO modulation is reductions of static stability (stability against convection) near the tropical tropopause, which tend to occur during the easterly phase of the QBO. Consistent with this possible cause, tropical lower stratospheric static stabilities have been declining since the most reliable observations began in the late 1970s. Here, it is shown that increased tropical upwelling rates resulting from long-term positive trends in early winter extratropical wave forcing of the stratospheric circulation have contributed significantly to the observed decline in tropical lower stratospheric static stability in boreal winter since that time. Increased sea level pressure anomalies over northern Eurasia produced by Arctic sea ice loss (and associated increases in Eurasian snow cover) can potentially explain the observed positive trends in early winter wave forcing. Climate model experiments are needed to test this possibility.

### 1. Introduction

The Madden-Julian Oscillation (MJO), also called the 40–50-day oscillation (Madden and Julian, 1994), is an eastward propagating pattern of tropical convection and precipitation that is a major driver of intraseasonal climate variability (for a recent review, see Jiang et al., 2020). In the tropics, the MJO has a steady circulation response that has characteristics of both a Kelvin and Rossby wave that shifts eastward with time (Adames & Kim, 2016). It releases a large amount of latent heat, which drives an extratropical Rossby wave train that propagates northward and eastward from its source in the subtropical western Pacific, affecting subseasonal climate at all latitudes and longitudes (e.g., Garfinkel et al., 2014; Hood et al., 2020; Zhang, 2013).

Recent research has identified several stratospheric influences on the MJO in boreal winter. Specifically, a primary influence of the stratospheric quasi-biennial oscillation on the MJO is well established (Nishimoto and Yoden, 2017; Yoo and Son, 2016; for reviews, see Jiang et al., 2020; Haynes et al., 2021; Martin, Son, et al., 2021). Also, a secondary influence of solar ultraviolet variations, which can modify stratospheric circulation, has been reported (Hoffmann and von Savigny, 2019; Hood, 2017, 2018). Attention is focused here on the primary quasi-biennial oscillation (QBO) influence.

The QBO is a major mode of internal stratospheric variability (Baldwin et al., 2001). It consists of a downward descending, oscillating variation of easterly and westerly tropical stratospheric zonal winds with a period averaging about 28 months. The phase of the QBO (easterly or westerly) varies continuously with altitude but is usually monitored at the 50 hPa level near the equator. The QBO-MJO relationship consists essentially of an enhancement and eastward continuation of MJO activity during the QBO's easterly phase (QBOE) relative to its westerly phase (QBOW). In contrast, no significant QBO modulation occurs for convectively coupled waves other than the MJO. Reasons for the uniqueness of the QBO-MJO connection are likely related to the higher vertical extent of MJO convection, as discussed by Abhik et al. (2019) and Sakaeda et al. (2020).

The effects of the QBO-MJO connection are not limited to the tropics. For example, the North Pacific storm track shifts poleward when MJO convection is located over the Indian Ocean and this shift has a larger amplitude in QBOE than in QBOW (Wang et al., 2018). In addition, the QBO modifies MJO-induced Rossby wave amplitudes at mid-to-high latitudes extending into the lower stratosphere (Hood et al., 2020; Roundy, 2022; Toms et al., 2020).

Although the QBO-MJO connection is robust in the observational record, climate models have struggled to simulate it (Domeisen et al., 2019; Kim et al., 2020; Martin, Orbe, et al., 2021). Despite the limitations of climate models, MJO forecasts are more skillful during QBOE largely due to the more systematic behavior of MJO convection (Abhik & Hendon, 2019; Lim et al., 2019; Lim and Son, 2020).

As reviewed by Martin, Son, et al. (2021) and Jiang et al. (2020), the physical mechanisms for the observed QBO and solar modulations of the MJO are incompletely understood. In the case of the QBO modulation, it has generally been hypothesized that QBO-induced changes in temperature and static stability in the tropical lowermost stratosphere and upper troposphere are the primary initiator of the connection. However, this is far from being a universally accepted fact. In particular, Martin, Orbe, et al. (2021) found using a nudging technique in climate model simulations that the modulation of static stability by the QBO was insufficient to simulate the QBO-MJO connection even when realistic QBO temperature perturbations were imposed in the model, questioning if static stability change is the key mechanism of the connection. Alternatively, this could reflect insufficient realism of other aspects of the model that were not nudged to observations, that is, the modeled MJO itself and/or several secondary processes and positive feedbacks. As reviewed recently by Son (2023), the latter include longwave cloud-radiative feedback within the MJO envelope in the upper troposphere (Sakaeda et al., 2020; Son et al., 2017) and a Kelvin-wave-like cold anomaly in the upper troposphere and lower stratosphere that enhances MJO eastward propagation across the Maritime Continent barrier (Hendon & Abhik, 2018; Kodera et al., 2023; Lim and Son, 2022). In any case, in the work reported here, it is implicitly assumed that the static stability change is the key initiating mechanism of the QBO-MJO connection.

One way that the QBO can alter lower stratospheric static stability is via the QBO mean meridional circulation in the tropics and subtropics (e.g., Yoo and Son, 2016), which produces relative equatorial upwelling in QBOE and downwelling in QBOW. This results in relative temperature and static stability decreases in QBOE in the tropical lowermost stratosphere. Since this mechanism would operate equally in all seasons, the occurrence of the QBO-MJO connection primarily in northern winter would be ascribed to a higher tropical tropopause during that season, especially over the Maritime Continent.

Another way that the QBO can affect temperature and static stability in the tropical lower stratosphere is via QBO influences on extratropical wave forcing of the stratospheric residual meridional circulation, the "Brewer-Dobson" circulation, or BDC (Hood, Trencham, & Galarneau, 2023; hereafter HTG23). Extratropical wave forcing in the Northern Hemisphere is mainly responsible for producing the climatological minimum in tropical lower stratospheric temperature that occurs near the middle of boreal winter (e.g., Randel et al., 2002). Extratropical planetary-scale Rossby waves have higher amplitudes in the Northern Hemisphere and can only propagate into the northern stratosphere near winter when stratospheric winds are westerly (Charney & Drazin, 1961). Absorption

and dissipation of these westward-propagating waves slows the westerly winds in the polar vortex, which, via the Coriolis torque, accelerates the BDC and the tropical upwelling rate. The wave forcing is stronger on average in early winter during QBOE than during QBOW, as was originally found for the November–December period by Holton and Tan (1980). This “Holton–Tan effect” in early winter therefore acts to further reduce tropical lower stratospheric static stabilities during QBOE as they are decreasing toward their climatological minima in mid-winter. The Holton–Tan effect changes sign in late boreal winter with stronger wave forcing on average during QBOW than during QBOE (Lu et al., 2020, and references therein). QBOE-induced cooling anomalies in the equatorial lower stratosphere are noticeably larger in boreal winter than in other seasons and are complemented by warming anomalies at high latitudes, implying an important role of extratropical wave forcing in producing the observed static stability reductions in QBOE (see, e.g., Figure 1 of HTG23). The Holton–Tan effect is not simulated well in current coupled climate models (e.g., Elsbury et al., 2021), due in part to lack of a sufficiently strong and continuous easterly QBO phase in most models.

Suggestive evidence for a role of extratropical wave forcing in producing the QBO–MJO connection has been obtained from studies of the effect of sudden stratospheric warmings (SSWs) on the MJO. SSWs are the most extreme examples of extratropical wave forcing events in the stratosphere (e.g., Butler et al., 2017; Charlton & Polvani, 2007). Previous work has found that certain phases of the MJO can favor the development of an SSW by deepening the Aleutian low and increasing the amplitudes of zonal wavenumber-one waves, which then propagate into the stratosphere and assist in breaking down the polar vortex (Garfinkel et al., 2012). However, recent work has found that the reverse can also happen: SSWs occurring in early winter can produce a lagged strengthening of the MJO (HTG23). Similar evidence for an enhancement of tropical convection by the 2019 Antarctic SSW has also been documented (Noguchi et al., 2020). SSWs occurring in early northern winter also produce more pronounced surface impacts at northern latitudes compared to SSWs occurring in late winter because the stratospheric polar vortex is stronger on average in early winter, requiring a larger polar vortex anomaly to reverse the zonal wind at 10 hPa, 60°N according to conventional SSW detection criteria (Monnin et al., 2021). If only strong QBOE and QBOW years are considered, SSWs in early winter (prior to ~January 15) occur mainly under QBOE conditions while those in late winter occur mostly under QBOW or QBO neutral conditions (see, e.g., Figure 3a of HTG23). SSWs do not usually occur in early winter under solar maximum conditions when the upper stratospheric westerly vortex is unusually strong, but tend to be delayed until late winter (e.g., Gray et al., 2004, 2020).

Several coupled climate models participating in the Coupled Model Intercomparison Project 6 (CMIP6) have been found to produce amplifications of the modeled MJO following early winter SSWs (HTG23; Hood, Trencham, Hoopes, & Galarneau, 2023). In the model simulations, those SSWs that produce the largest reductions in static stability in the tropical lower stratosphere (70–100 hPa) also produce the largest lagged strengthenings of the MJO. This is evidence that top-down forcing of tropical lower stratospheric static stability reductions, at least by SSWs, can strengthen the MJO, at least in some CMIP6 models.

Finally, several recent studies have proposed that the QBO–MJO connection has strengthened significantly in observational records since the early 1980s. Using reconstructed MJO and QBO indices dating back to 1905, Klotzbach et al. (2019) found that the connection was not statistically significant prior to ~1980. They noted that the apparent emergence of the relationship after this time coincides with a cooling trend in the equatorial lower stratosphere and a warming trend in the upper troposphere, which would act to increase the sensitivity of MJO convective activity to QBO-induced static stability decreases near the tropopause. They also showed evidence that the enhanced Kelvin-wave-like cold anomaly during QBOE mentioned above was stronger after 1980 than before this time. In a separate study, Sakaeda et al. (2020) calculated MJO convective activity from MJO-filtered outgoing longwave radiation data from the JRA-55 reanalysis over the 1958 to 2017 period. They found no apparent relationship between MJO convective activity and the QBO between 1958 and 1978 but a strong relationship after this time. If these conclusions are correct, then an increasing QBO (and solar) modulation of the MJO will be superposed on expected increases in MJO-related precipitation intensity under anthropogenic warming (e.g., Maloney et al., 2019; Zhou et al., 2020).

In this paper, the evolution with time of the QBO–MJO connection is investigated further. After describing the data and methods in Section 2, the temporal evolution of the boreal winter QBO–MJO connection over the 1959 to 2021 period is investigated further in Section 3 together with associated interannual and longer-term variations of tropical static stability and extratropical wave forcing in early winter. Attention is focused on lower stratospheric (70–100 hPa) static stability in boreal winter (DJF) because it is found to correlate much better with interannual

variations of DJF mean MJO amplitude caused by the QBO than does upper tropospheric (100–200 hPa) static stability. During the most reliable (post-satellite) part of the observational record beginning in 1979, a high inverse correlation is obtained between early winter extratropical wave forcing anomalies and DJF mean tropical lower stratospheric static stability. In Section 4, a simplified analytic model based on the Eulerian mean thermodynamic energy equation is used to show that most of the tropical lower stratospheric temperature reduction at 70 hPa during a winter with strong early winter wave forcing (2003–2004) can potentially be explained as due to the observed increase in extratropical wave forcing in late fall and early winter. This supports a contribution from extratropical wave forcing to interannual variations of wintertime static stability in the 70 to 100 hPa layer because the latter variations are dominantly determined by interannual temperature variations at the 70 hPa level. In Section 5, regression relationships between interannual changes of early winter wave forcing and tropical lower stratospheric temperature and static stability are therefore applied to estimate the degree to which observed positive trends in early winter wave forcing since the late 1970s can contribute to the observed negative static stability trends after this time. In Section 6, previous work reporting evidences for positive trends in SSWs since 1980 and for a role of Arctic sea ice loss (and associated increases in Eurasian snow cover) in producing those trends via effects on sea level pressure are briefly reviewed. This is followed by an investigation of sea level pressure anomaly differences between the first and second halves of the period since 1979. A summary and discussion are given in Section 7.

## 2. Data and Methods

With a few exceptions necessitated by the longer data record, the data and methods used here follow closely those previously described in HTG23. Briefly, all observational data for atmospheric variables are taken from the ERA5 reanalysis record (Hersbach et al., 2020) and its recently completed back-extension to 1959 (Bell et al., 2021). The outgoing longwave radiation (OLR)-based MJO index (OMI) developed by Kiladis et al. (2014) is adopted to characterize MJO amplitude. This index is based on satellite OLR data and is provided since 1979 on a NOAA website: <https://psl.noaa.gov/mjo/mjoindex/>. Its amplitude is normalized such that  $OMI = 1.0$  represents one standard deviation. Prior to 1979 when continuous satellite OLR data are unavailable, the ERA5 reanalysis OLR data are adopted to calculate OMI indices. This is done using a Python computer code package, “mjoindices,” available from <http://dx.doi.org/10.5281/zenodo.3613752> (Hoffmann et al., 2021). Briefly, the package first filters daily 20°S to 20°N OLR values to accept only eastward propagation in the period range of 30–96 days. It then projects the 20–96 days filtered OLR values onto the two leading-order empirical orthogonal functions for each calendar day that are calculated from the ERA5 daily OLR data during 1979–2021. EOFs from this time period are used to ensure consistency with the NOAA OMI data after 1979.

The directly measured (radiosonde) equatorial 50 hPa zonal wind monthly means ( $u_{50}$ ) compiled at the Free University of Berlin are employed to determine the phase of the QBO. Strong QBOE and QBOW years are identified using the “strict” criteria described in HTG23 (briefly,  $u_{50}$  mean winds during October to January differing from zero positively by more than 0.6 standard deviations or negatively by more than  $-1$  standard deviations and changing sign no later than August).

In order to characterize extratropical wave forcing, the zonal mean meridional eddy heat flux ( $\overline{v'T'}$ ) at 100 hPa is calculated at a daily cadence and averaged over 45°N to 75°N. As discussed in Section 3, daily static stabilities are calculated for two near-tropopause layers, the 70 to 100 hPa layer in the lowermost stratosphere and the 100 to 200 hPa layer in the uppermost troposphere. These static stabilities are calculated using methods described in Hood (2017) and are averaged over near-equatorial latitudes (10°S to 10°N).

Finally, central dates of SSWs occurring during the study period (1959–2021) are selected based on compilations given by Charlton and Polvani (2007), Butler et al. (2017), and Karpechko (2018). In addition, three more recent SSW central dates are included occurring on 12 February 2018, 2 January 2019, and 5 January 2021 (Davis et al., 2022; Rao et al., 2019).

## 3. Temporal Evolution of the QBO-MJO Connection: 1959–2021

In this section, the temporal evolution of the QBO-MJO connection in boreal winter and its relationship to tropical static stability variations are investigated using ERA5 data for the 1959 to 2021 period. The relationship of the tropical static stability variations to extratropical wave forcing in early winter is also investigated.

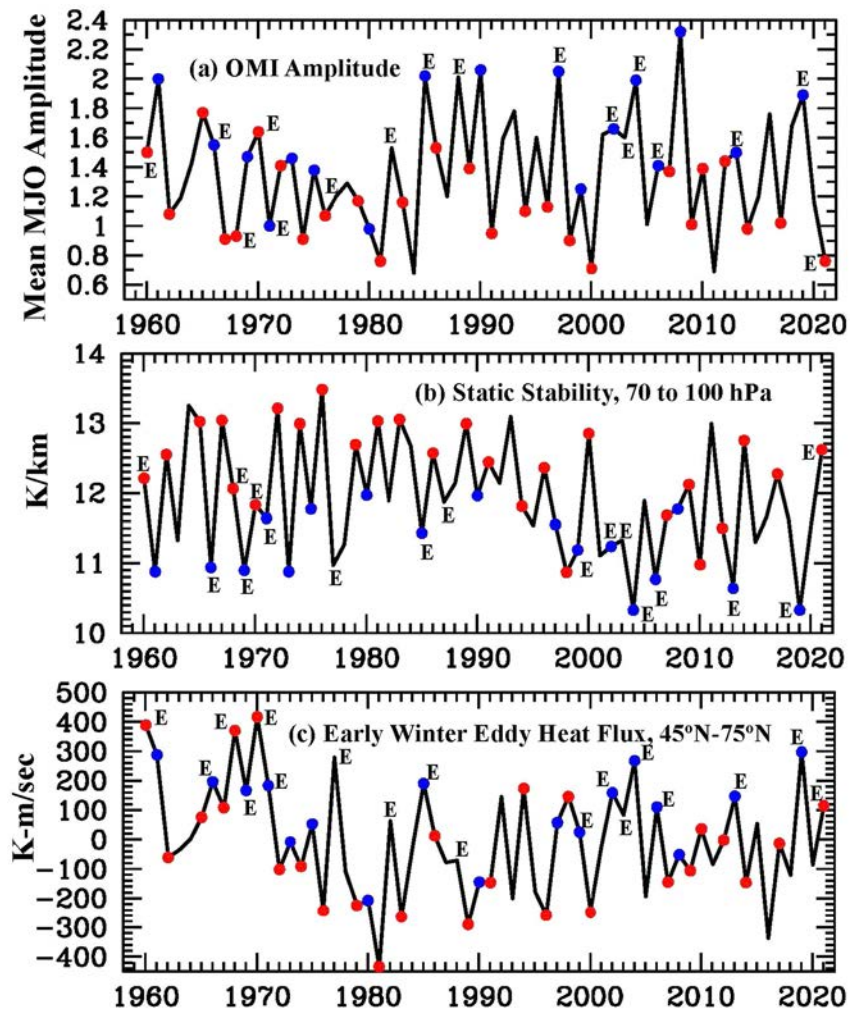


**Figure 1.** (a) Northern winter (DJF) mean MJO amplitude; (b) DJF mean static stability (70–100 hPa; 10°S to 10°N); and (c) cumulative 100 hPa eddy heat flux anomalies at northern midlatitudes during early winter. Blue symbols indicate years that were in a strong easterly QBO phase; red symbols indicate years that were in a strong westerly QBO phase. Years when a sudden stratospheric warming occurred in early winter (prior to January 21) are labeled “E”.

Figure 1a shows a time series of DJF mean MJO amplitude for 62 winters. As described in Section 2, amplitudes are calculated from ERA5 OLR data prior to 1979 and the NOAA-provided daily OMI amplitudes are used after this time. Winters that qualified as strongly QBOE or QBOW are identified by blue and red symbols, respectively. Note that the 2020–2021 winter is accepted as a strong QBOW winter even though it slightly failed the selection criteria (the  $u_{50}$  wind only changed to westerly in September of that year although it was strong afterward throughout the winter). Winters in which a sudden stratospheric warming (identified using conventional criteria, see below) occurred during early winter (prior to January 21) are labeled “E.” Overall, QBOE years are characterized by higher DJF mean MJO amplitudes than QBOW years but the difference appears to increase starting in the early 1980s. As noted in the Introduction, early winter SSWs occurred mainly during QBOE years although exceptions occurred in 1960, 1970, and 2021. Interannual variability associated with the QBO becomes stronger after the early 1980s, consistent with the results of Klotzbach et al. (2019) and Sakaeda et al. (2020), who used different data sources.

Figure 1b shows a similar time series of tropical lower stratospheric (70–100 hPa) static stability, zonally averaged from 10°S to 10°N. Overall, static stabilities in this layer are larger during QBOW years than during QBOE years, as indicated by the red and blue symbols. As discussed in the Introduction, this is indicative of increased tropical upwelling due to a combination of the QBO induced meridional circulation and extratropical wave forcing of the mean meridional (Brewer-Dobson) circulation. Early winter SSWs therefore correlate closely with

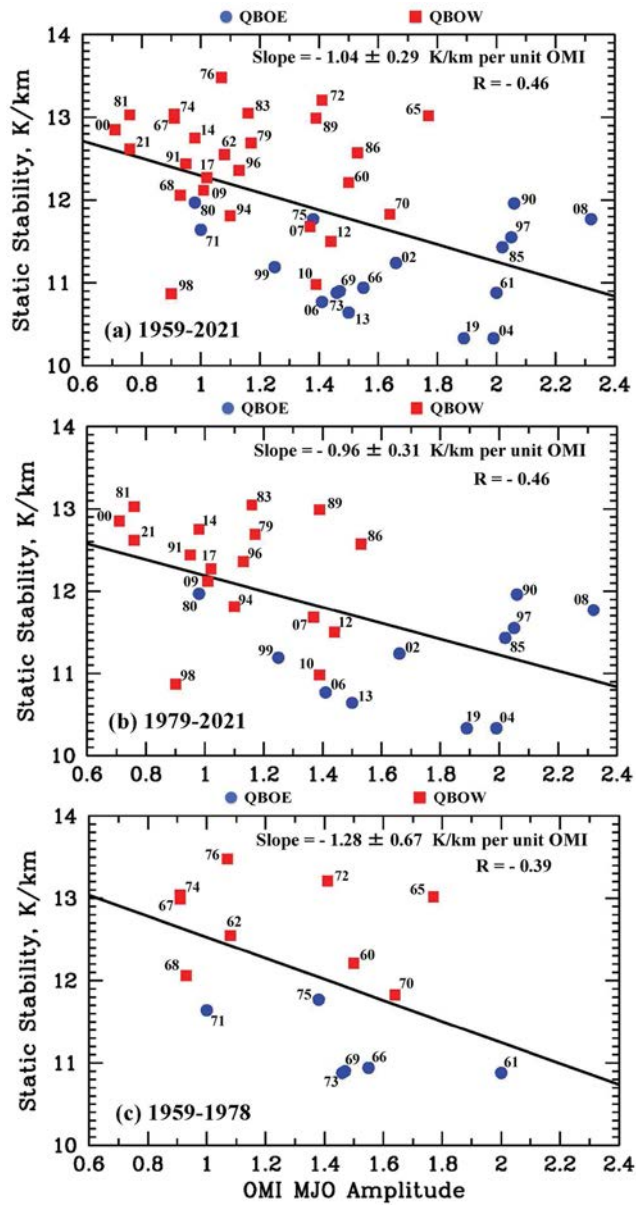


**Figure 2.** Northern winter (DJF) mean static stability (70–100 hPa; 10°S–10°N) versus DJF mean MJO amplitude for strong QBOE years (blue symbols) or QBOW years (red symbols). (a) All years in 1959–2021; (b) years after 1979; (c) years before 1979.

low static stability winters. A long-term mean decrease in static stability occurs in the second half of the record, especially after 1990. Figure S1a in Supporting Information S1 shows a time series of tropical upper tropospheric (100–200 hPa) static stability, also zonally averaged from 10°S to 10°N. In this layer, interannual variability of static stability is weaker than for the 70 to 100 hPa layer but there is a more continuous downward trend with time, especially after the middle 1970s.

Figure 1c is a corresponding time series of early winter zonal mean eddy heat flux ( $\overline{v'T'}$ ) at northern midlatitudes (i.e., cumulative daily eddy heat flux anomalies at 100 hPa averaged over 45°N to 75°N and summed from October 1 to January 15 in each winter).  $\overline{v'T'}$  is approximately proportional to the vertical component of the planetary wave flux and so provides a reasonable measure of the amplitude of extratropical wave forcing of the stratospheric polar vortex. Early winters with high eddy heat fluxes occur more often during QBOE years than during QBOW years. This is consistent with the Holton-Tan effect reviewed in the Introduction. Notable exceptions are seen in 1960, 1968, and 1970 when high eddy heat fluxes occurred in early winter during strong QBOW years. Early winter SSWs (“E” labels) tend to coincide with high eddy heat flux years, as would be expected.

Figure 2a is a scatterplot of DJF mean equatorial static stability in the 70 to 100 hPa layer (from Figure 1b) versus DJF mean OMI MJO amplitude (from Figure 1a) for those winters in 1959–1960 to 2020–2021 that qualified as strong QBOE and QBOW years. Numbers beside each symbol indicate the winter that is plotted (e.g., “67” is the 1966–1967 DJF winter). Slopes of least-squares-fitted regression lines and one standard deviation errors of the slopes are given on the figure. As indicated by the regression line, a quasi-linear relationship is obtained with a negative slope that differs significantly from zero by more than two standard deviations. The overall correlation coefficient is  $-0.46$  and is significant at 95% confidence. Most QBOE years are in the lower right (indicating lower static stability and higher MJO amplitude) while most QBOW years are in the upper left (higher static stability and lower MJO amplitude). This negative correlation and division by QBO phase was first shown by Yoo and Son (2016; see their Figure 4b), who interpreted it as evidence in favor of the effect of the QBO induced meridional circulation on static stability near the tropopause with downward influence on the MJO. As argued by HTG23, the effect of the induced meridional circulation on tropical static stability in this layer is augmented substantially by increased tropical upwelling in QBOE driven by the Holton-Tan effect in boreal winter. In contrast, as shown in Figure S1b in Supporting Information S1, a similar scatterplot of DJF mean equatorial static stability in the 100 to 200 hPa layer versus DJF mean OMI amplitude yields a correlation coefficient of only  $-0.23$  and a regression line slope of  $-0.25 \pm 0.19$  K/km per unit OMI, which is not significant. This confirms that the QBO modulates lower stratospheric static stability much more strongly than upper tropospheric static stability, as would be expected.

In the remainder of Figure 2, the same regression analyses are done for (b) the 1978–1979 to 2020–2021 winters; and (c) the 1959–1960 to 1977–1978 winters. For the former period, the QBOE and QBOW years remain well separated in MJO amplitude and the regression line slope differs from zero by more than three standard deviations. For the latter period, this is not the case and there is only a marginal tendency for QBOE years to have higher MJO amplitudes than QBOW years. This is again consistent with the results of Klotzbach et al. (2019) and Sakaeda et al. (2020). While static stabilities are generally lower for QBOE years than for QBOW years during 1959–1978, the mean static stabilities during both QBO phases are somewhat higher than during 1979–2021, consistent with the weaker MJO amplitude difference. Also, as discussed further below, several QBOW years

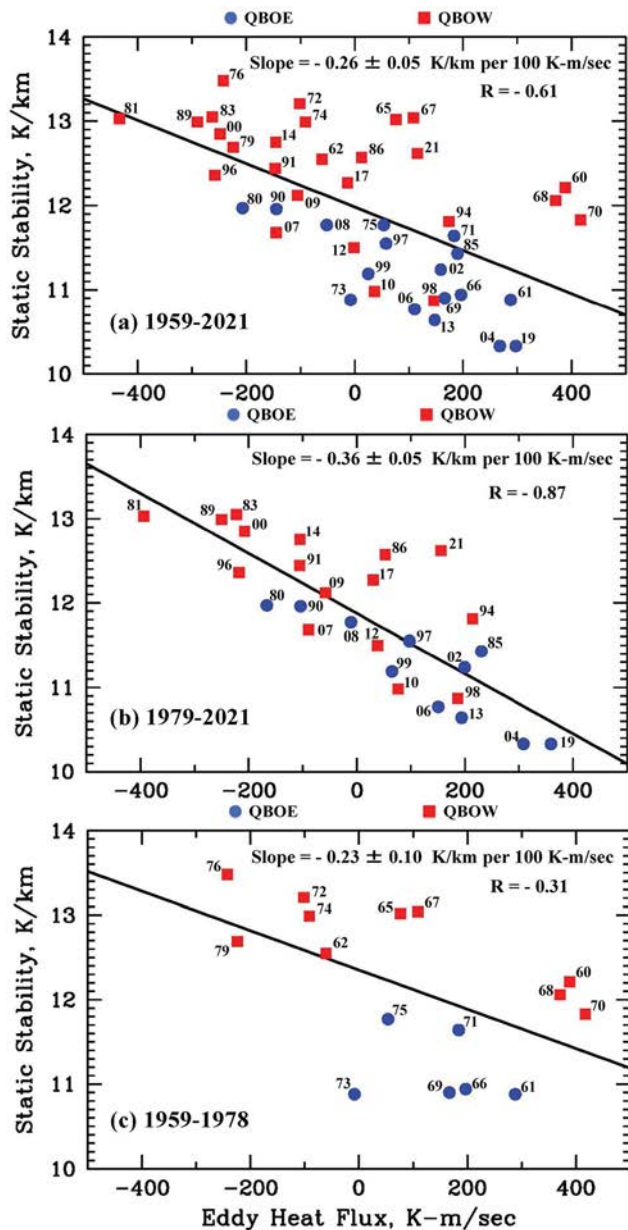


**Figure 3.** As in Figure 2 but for DJF mean static stability (70–100 hPa; 10°S–10°N) versus early winter cumulative eddy heat flux anomalies at northern midlatitudes.

during 1959–1978 had anomalously low static stabilities, contributing to the weaker QBO-MJO connection.

Figure 3a shows regression and correlation analyses similar to those of Figure 2a but using early winter eddy heat fluxes from Figure 1c as the independent variable. Again, only years that qualified as strong QBOE or QBOW years are plotted (43 of 62 years). A correlation coefficient of  $-0.61$  and a very significant regression line slope of  $-0.26 \pm 0.05$  K/km per 100 K-m/sec are obtained. As shown in Figures 3b and 3c only the period after 1979 is considered, the correlation increases to  $-0.87$  and the regression line slope increases to  $-0.36 \pm 0.05$  K/km per 100 K-m/sec. For times prior to 1979 (Figure 3c), the correlation coefficient and regression line slope are reduced to  $-0.31$  and  $-0.23 \pm 0.10$ , which is barely significant at the two standard deviation level. Much of the reduced correlation in the latter period is due to the 1959–1960, 1967–1968, and 1969–1970 winters, which were quite anomalous in having high early winter wave fluxes and early winter SSWs during strongly QBOW years. During these winters, static stabilities were therefore lower than usual for QBOW years but higher-than-expected for high early winter-wave-flux years. An examination of the temporal evolution of relevant quantities for these years shows that 70 hPa tropical temperatures and lower stratospheric static stabilities start out anomalously high, possibly because of the QBO induced meridional circulation, so mid-winter static stabilities never reach levels below climatological means (see Figure S2 in Supporting Information S1 for a plot of the 1959–1960 winter). If these years are removed from Figure 3c, correlation coefficients and regression line slopes become comparable to those of Figure 3a. Overall, Figure 3 indicates that DJF mean tropical static stabilities were much more sensitive to early winter extratropical wave forcing during the period after 1979. This may be partly because of higher data quality in the post-satellite part of the record or it may be because of anomalous years in the early part of the record, or both.

#### 4. 70 hPa Temperature Reductions in Mid-Winter: A Simplified Model

As found in the previous section (Figure 2a; Figure S1b in Supporting Information S1), static stability in the tropical lowermost stratosphere (70–100 hPa) correlates better with interannual changes in DJF mean MJO amplitude than does static stability in the uppermost troposphere (100–200 hPa). As shown in Figure S3 in Supporting Information S1, interannual variability and long-term trends in 70–100 hPa tropical static stability are dominantly due to variability of the 70 hPa temperature time series. In this section, a case study of a specific winter is conducted and a simplified analytic model is applied to show that the reduction of 70 hPa temperature to its midwinter minimum during that year can be largely explained by the cumulative effects of extratropical wave forcing.

Figure 4 plots the temporal evolution of a series of relevant quantities during 2003–2004 when the QBO was in a strongly easterly phase, the boreal winter static stability was unusually low, and the MJO amplitude was unusually high (cf. Figures 1 and 2). The top panel (a) plots the zonal mean meridional eddy heat flux ( $\overline{v'T'}$ ) at 100 hPa, averaged over 45°N to 75°N. The second panel (b) plots the daily zonal mean temperature at 70 hPa averaged over polar latitudes (66°N to 90°N) while the third panel (c) plots the same quantity averaged over equatorial latitudes (10°S to 10°N). The fourth panel (d) plots daily zonal mean 70 to 100 hPa static stability averaged over equatorial latitudes while the fifth panel (e) plots the daily MJO OMI amplitude. All plotted quantities (blue lines) are compared to their climatological means (dashed lines).

As indicated by the vertical bar in Figure 4b, an SSW occurred with central date on 5 January 2004. It was preceded by a strong increase in extratropical wave forcing as shown in the top panel. As reviewed in the

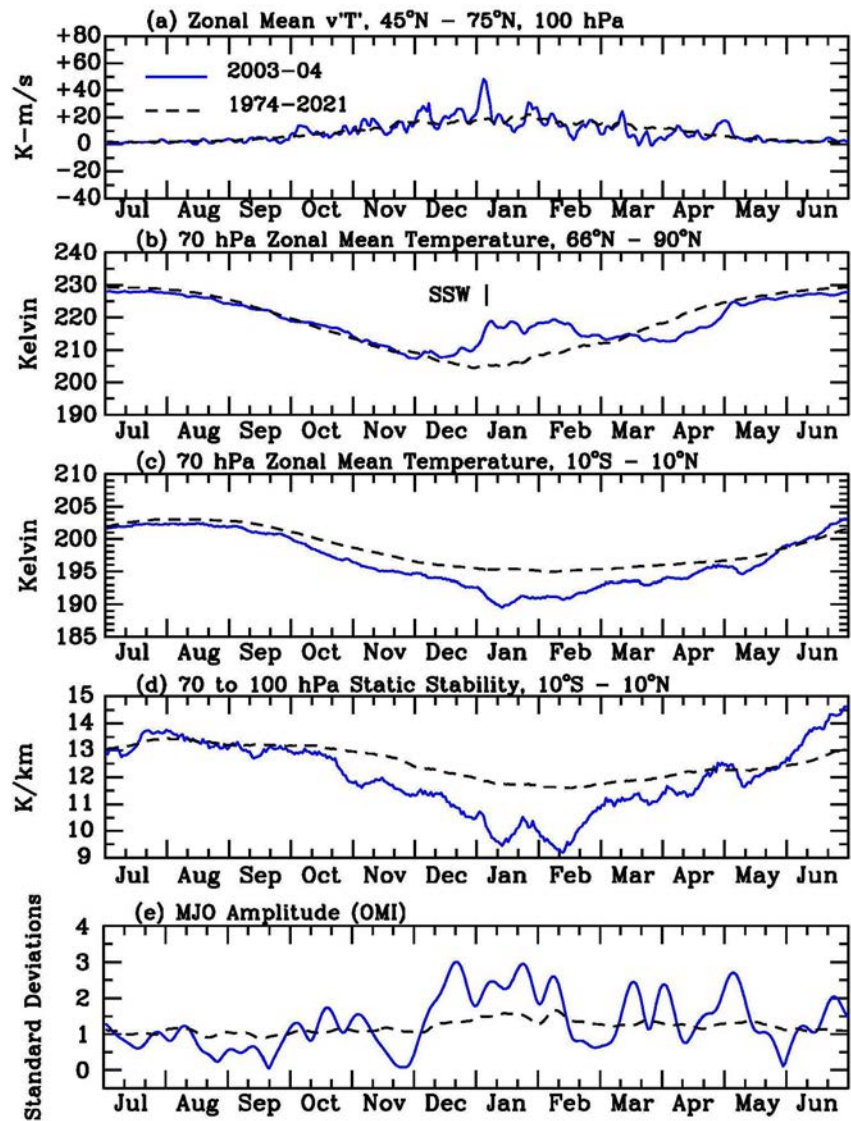


**Figure 4.** Daily mean time series for 2003–2004 centered on northern winter of (a) meridional eddy heat flux at northern midlatitudes; (b) zonal mean temperature at 70 hPa at high northern latitudes; (c) same as (b) but at tropical latitudes; (d) tropical lower stratospheric static stability; and (e) MJO amplitude. Dashed lines are climatological means.

Introduction, there is evidence from both observations and climate model simulations for a strengthening of the MJO on average following SSWs in early winter. However, during this year, the equatorial lower stratospheric temperatures (Figure 4c) and static stability (Figure 4d) were already low in November and December, and the MJO amplitude (Figure 4e) was already high in December. As seen in Figure 4a, extratropical wave forcing was also above average during several periods in October, November, and December prior to the large increase in early January. Increased early winter wave forcing is commonly observed in QBOE (the Holton-Tan effect).

A number of prior studies have found that extratropical wave forcing of the polar vortex and the BDC is a primary determinant of zonal-mean temperatures in the tropical lower stratosphere on both seasonal (Randel et al., 2002) and longer-term (Fueglistaler et al., 2014) time scales. In order to investigate quantitatively whether the increased early winter wave forcing in Figure 4a could be the primary cause of the reduced equatorial 70 hPa temperatures and 70 to 100 hPa static stabilities for 2003–2004 seen in Figures 4c and 4d, it is useful to consider a simplified version of the thermodynamic energy equation in the transformed Eulerian mean (TEM) formulation (e.g., Andrews et al., 1987). Similar approaches have been applied by previous authors (Fueglistaler et al., 2014; Hood & Soukharev, 2003; Randel et al., 2002). In general, the TEM thermodynamic energy equation may be written as

$$\frac{\partial \bar{T}}{\partial t} + \frac{\bar{v}^*}{a} \frac{\partial \bar{T}}{\partial \varphi} + \bar{w}^* \left( \frac{HN^2}{R} \right) = \bar{Q} \quad (1)$$

where  $t$  is time,  $\varphi$  is longitude,  $\bar{v}^*$  and  $\bar{w}^*$  are TEM meridional and vertical velocities,  $a$  is the Earth's radius,  $\bar{T}$  is zonal mean temperature at 70 hPa averaged over 10°S to 10°N,  $H$  is scale height,  $R$  is the dry air gas constant, and  $\bar{Q}$  is the zonal mean diabatic heating rate. Neglecting heat transport by meridional winds compared to vertical winds and neglecting short-wave heating compared to long-wave cooling, Equation 1 may be written in the simplified form (e.g., Randel et al., 2002),

$$\frac{\partial \bar{T}}{\partial t} \cong -\bar{w}^* \left( \frac{HN^2}{R} \right) - \left( \frac{\bar{T} - \bar{T}_{\text{eq}}}{\tau_r} \right) \quad (2)$$

where a Newtonian cooling approximation has been assumed with equilibrium temperature  $\bar{T}_{\text{eq}}$  and radiative lifetime  $\tau_r$ .

Previous estimates for the magnitude of  $\tau_r$  in the lower stratosphere range from  $\sim 30$  days (e.g., Hartmann et al., 2001; Newman and Rosenfield, 1997) to  $\sim 100$  days (e.g., Fueglistaler et al., 2014; Kiehl & Solomon, 1986; Mlynczak et al., 1999). For temperature changes resulting from tropical upwelling associated with short-term ( $< 15$  days) wave absorption events, the radiative term on the right side of Equation 2 is small and can be approximated as a constant relaxation rate,  $C$ .

As discussed for example, by Hood and Soukharev (2003; their Section 4),  $\overline{v'T'}$  is approximately proportional to the net force per unit mass of extratropical wave forcing on the zonal mean flow. Acceleration of the extratropical flow accelerates the Brewer-Dobson circulation which, in turn, increases the tropical upwelling rate. Therefore, for short-term extratropical wave absorption events (e.g., those associated with SSWs),  $\bar{w}^*$  in the Tropics can be assumed to be approximately proportional to  $\overline{v'T'}$  averaged over 45°N to 75°N. Denoting the latter quantity as  $F_z$ , Equation 2 reduces to

$$\frac{\partial \bar{T}}{\partial t} \cong -B F_z - C \quad (3)$$

where  $B$  and  $C$  are constants which can be estimated empirically from observed short-term variations of  $F_z$  and  $\bar{T}$ .

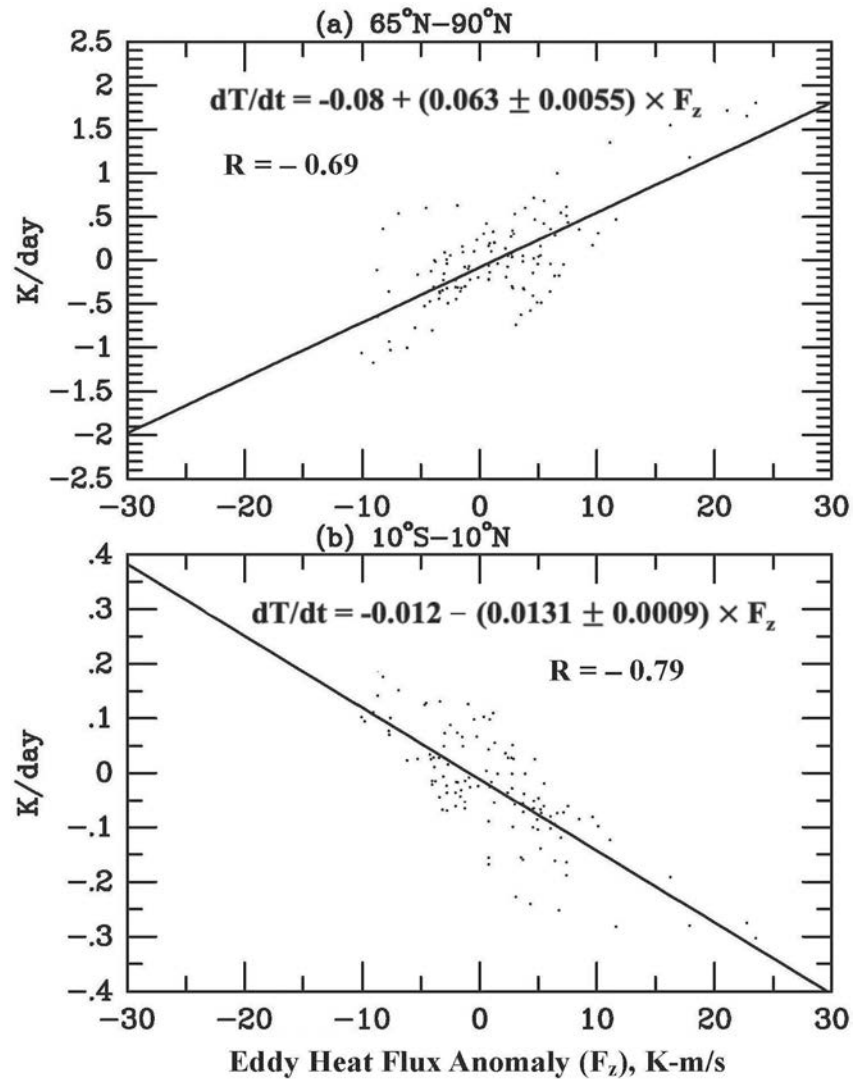
Figure S4 in Supporting Information S1 plots daily 70 hPa temperature tendencies in the extratropics (65°N to 90°N) and equatorial zone (10°S to 10°N) during November to April of 2003–2004. To calculate these tendencies, the zonal mean, latitudinally averaged, 70 hPa temperature time series were first smoothed using a 5-day running boxcar filter. Then temperature tendencies on a given day were estimated by subtracting the smoothed temperatures on the day before from those on the day after and dividing by two. For comparison, Figure S4c in Supporting Information S1 plots  $F_z$  anomalies (deviations from climatological means) after 5-day smoothing during the same time period. Positive correlations between the  $F_z$  anomalies and the extratropical temperature tendencies (Figure S4a in Supporting Information S1) are visually evident. Negative correlations are obtained for the tropical tendencies (Figure S4b in Supporting Information S1).

Figure 5 shows scatter plots and regression results for the November to February part of Figure S4 in Supporting Information S1 when the largest variations were observed. Correlation coefficients ( $-0.69$  for 65°N–90°N and  $-0.79$  for 10°S–10°N) are relatively high for this time period reflecting a dominant role during this winter of northern hemispheric extratropical wave forcing events in determining 70 hPa temperature variability. Not all winters yield such high correlations due to other sources of variability. Comparing the regression results of Figure 5b with Equation 3, the estimated values of the coefficients are  $B = 0.013$  and  $C = 0.012$ .

For temperature variations occurring over an entire season, the radiative term on the right side of Equation 2 is no longer negligible. The temperature tendency on this time scale can then be written as

$$\frac{\partial \bar{T}}{\partial t} \cong -B F_z - C - \left( \frac{\bar{T} - \bar{T}_{\text{eq}}}{\tau_r} \right) \quad (4)$$

The red curve in Figure 6b shows the result of integrating Equation 4 forward in time beginning on October 1 and using the daily values of  $F_z$  plotted in Figure 6a. The equilibrium temperature  $\bar{T}_{\text{eq}}$  is taken to be equal to the



**Figure 5.** Daily 70 hPa temperature tendencies for November to February of 2003–2004 plotted versus corresponding daily zonal mean meridional eddy heat flux anomalies (deviations from long-term means) at 100 hPa averaged over 45°N to 75°N. Temperature tendencies are averaged over (a) 65°N to 90°N; and (b) 10°S to 10°N.

initial value of  $\bar{T}$  (199.6 K). Repeating the calculation over the October to April period iteratively for trial values of  $\tau_r$  yields a minimum variance fit (RMS = 0.55 K) for  $\tau_r = 33$  days, which lies within the range of previous estimates given above.

While simplified, this model calculation demonstrates that much of the temperature decline to a minimum in northern winter in the tropical lower stratosphere can be attributed to increases in extratropical wave forcing occurring in early winter. After midwinter (mid to late January) when  $F_z$  begins decreasing, 70 hPa tropical temperatures begin increasing again toward  $\bar{T}_{eq}$ .

## 5. Trends in Early Winter Wave Forcing and Tropical Static Stability Since 1979

Considering the increased reliability of the data record since the late 1970s when continuous satellite remote sensing data became available, attention is focused in this section on observed trends in tropical lower stratospheric DJF mean static stability and early winter eddy heat flux since that time. The objective is to evaluate whether trends in the latter can explain a significant part of trends in the former, thereby potentially contributing to the observed strengthening of the QBO-MJO connection during this period.

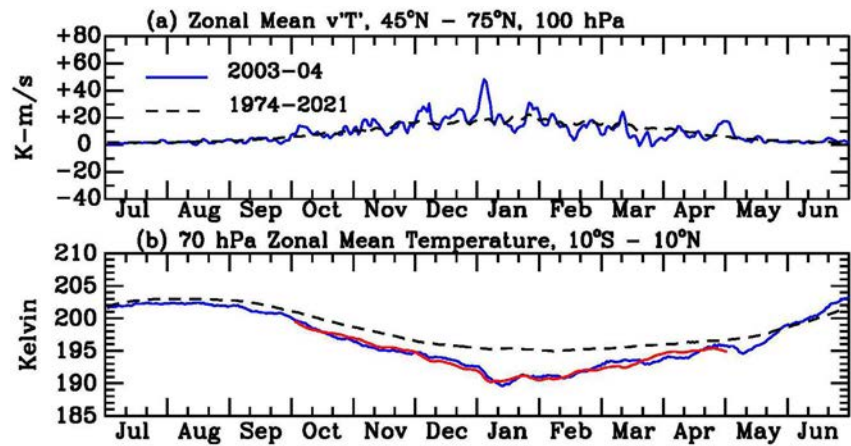


**Figure 6.** As in Figures 4a and 4d but comparing the observed tropical lower stratospheric temperature time series (b) with a model time series (red line) calculated from the observed eddy heat flux time series (a) using the observed sensitivity of 70 hPa temperature tendencies to eddy heat flux anomalies (Figure 5b). See the text.

Figure 7a reproduces the DJF mean MJO amplitude time series of Figure 1a for the 1975 to 2021 period. Superposed regression lines for QBOE years (blue) and QBOW years (red) diverge with time, consistent with a strengthening of the modulation (see also Figure 3 of Klotzbach et al., 2019). Figure 7b reproduces the time series of Figure 1b for the 1975 to 2021 period. Regression line slopes are significantly negative for the QBOE years ( $-0.33 \pm 0.09$  K/km per decade), for all years ( $-0.18 \pm 0.08$  K/km per decade), and nearly so for QBOW years ( $-0.24 \pm 0.14$  K/km per decade). Although trends for all years are negative, there is no appreciable increase in mean MJO amplitude with time as seen in Figure 7a (black dotted line). However, the stronger negative trend in static stability for QBOE years in Figure 7b may have acted to strengthen the QBO modulation with time if the increase in DJF mean MJO amplitude during QBOE years was more sensitive to reductions in lower

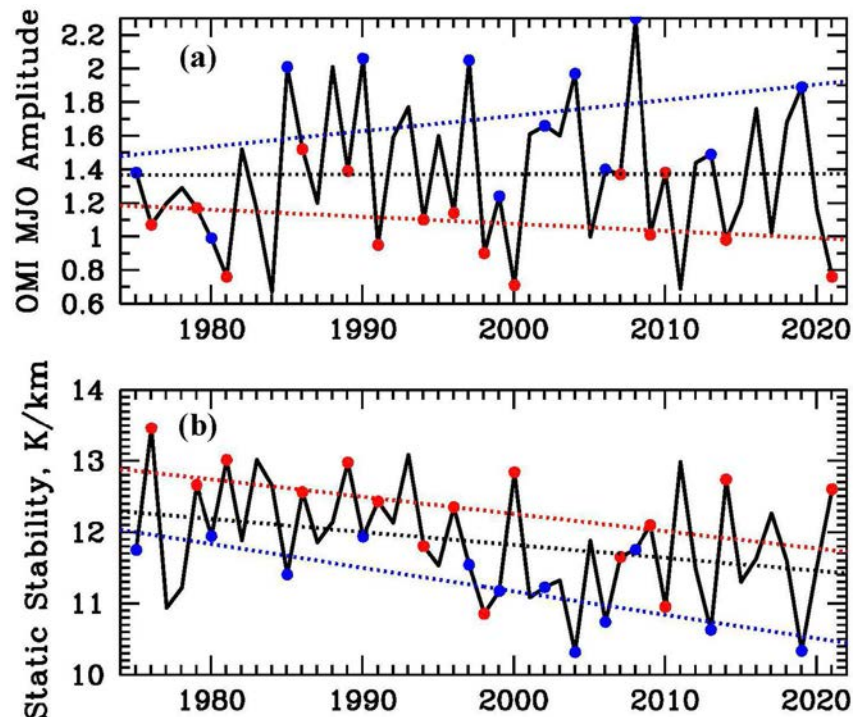


**Figure 7.** Same data as in Figures 1a and 1b but for the 1975 to 2021 period. Regression lines are for all years (black), strong QBOE years (blue), and strong QBOW years (red).

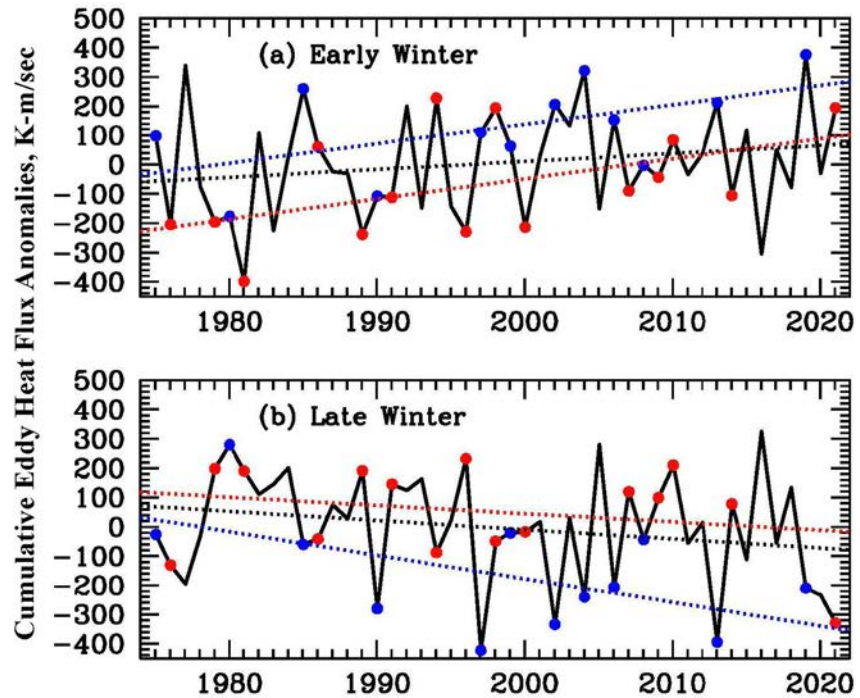


**Figure 8.** Same format as Figure 7 but for (a) early winter extratropical wave forcing anomalies (same data as in Figure 1c) and (b) late winter anomalies. See the text for the definitions of early and late winter.

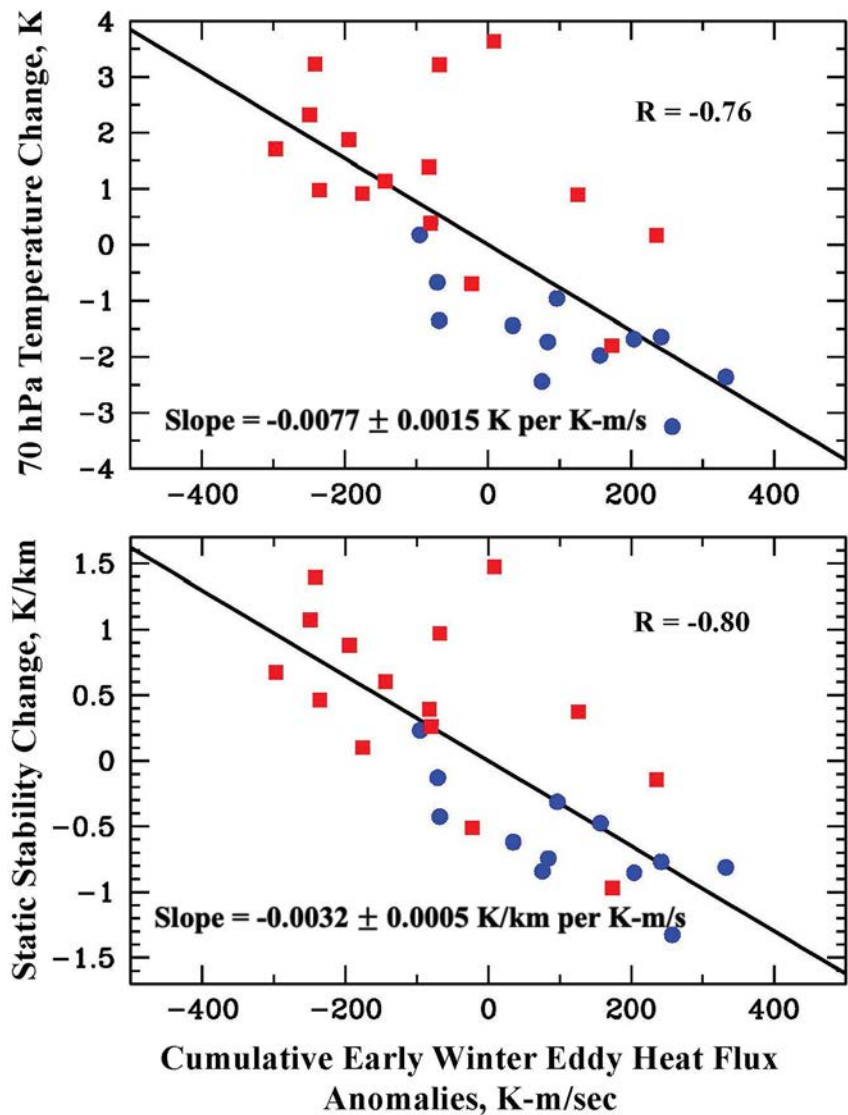
stratospheric static stability than were the decreases that occurred during QBO years. This would be possible if the sensitivity increased with decreasing static stability, for example. In addition, as also pointed out by Klotzbach et al. (2019), the more rapid decrease in upper tropospheric static stability since the 1970s (Figure S1a in Supporting Information S1) may have acted to increase the sensitivity of MJO amplitude to QBO-induced static stability reductions in the lowermost stratosphere.

Figure 8a reproduces the early winter eddy heat flux time series of Figure 1c for the 1975 to 2021 period with the addition of regression lines as in Figure 7. Specifically, it plots time series starting in 1975 of extratropical (45°N–75°N) meridional eddy heat flux anomalies (deviations from daily climatological means) summed over the early winter period of October 1 to January 15. Figure 8b plots a similar time series for the late winter period of January 16 to April 30. Years of strong QBOE and QBOW conditions are again indicated by blue and red symbols. In Figure 8a (early winter), a majority of the strong QBOE years have larger cumulative early winter anomalies than do strong QBOW years. In Figure 8b (late winter), the opposite is true, consistent with a change-of-sign of the Holton-Tan effect in late winter compared to early winter (e.g., Lu et al., 2020).

In both parts of Figure 8, dotted lines represent linear regression fits to the full 47-winter record (black), QBOE years only (blue), and QBOW years only (red). In early winter (Figure 8a), the two regression lines for QBOE and QBOW years have positive slopes and are statistically significant ( $6.7 \pm 3.3$  K-m/s per year and  $6.9 \pm 3.4$  K-m/s per year, respectively). In late winter (Figure 8b), only the regression line for strong QBOE years (blue dotted line) has a statistically significant negative slope ( $-8.1 \pm 3.9$  K-m/s per year). If cumulative heat flux anomalies are calculated for the entire winter (October 1 to April 30), no significant slopes are obtained (not shown).

As found in the previous section, extratropical wave forcing ( $F_2$ ) occurring in early winter can potentially determine the depth of the 70 hPa tropical lower stratospheric temperature minimum in mid-winter, at least in some years. It is therefore of interest to investigate whether the positive trends in cumulative early winter wave forcing in Figure 8a can contribute to explaining the observed decreasing trends since the late 1970s in tropical 70 hPa DJF temperature (Figure S3a in Supporting Information S1) and 70 to 100 hPa DJF static stability (Figure 7b).

For this purpose, it is first necessary to have a measure of the sensitivity of tropical 70 hPa temperature and 70 to 100 hPa static stability in DJF to interannual changes in cumulative early winter eddy heat flux anomalies.



**Figure 9.** (a) DJF mean 10°S to 10°N 70 hPa zonal mean temperature interannual deviations for strong QBOE (blue) and QBOW (red) years plotted versus cumulative early winter eddy heat flux anomaly interannual deviations. (b) As in (a) but for DJF mean 10°S to 10°N 70 to 100 hPa static stability interannual deviations.

Several approaches toward estimating this sensitivity are possible. One approach is to take the 2003–2004 winter considered in the previous section and extrapolate those results to all years. For this particular year, as plotted in Figure 8a, the cumulative early winter eddy heat flux anomaly was ~310 K-m/s. The mean 70 hPa DJF temperature reduction relative to the long-term mean plotted in Figure 7b was ~–3.5 K, leading to an estimated sensitivity of ~0.011 K per K-m/s. However, this value is more of an upper limit because, in 2003–2004, a major early winter SSW occurred under QBOE conditions, which produced an especially strong tropical temperature and static stability reduction. In other years, other sources of variability (e.g., ENSO) result in less sensitivity of the mid-winter 70 hPa temperature minimum to early winter wave forcing.

A better approach is therefore to estimate interannual changes in all quantities for multiple years by subtracting the linear trend regression lines from the time series of cumulative early winter eddy heat flux (Figure 8a), tropical 70 hPa temperature (Figure S3a in Supporting Information S1), and 70 to 100 hPa static stability (Figure 7b). Only strong QBOE and QBOW years, which have the most significant slopes, are considered. Figure 9 plots the resulting interannual deviations of tropical 70 hPa temperature and 70 to 100 hPa static stability against the cumulative eddy heat flux anomaly interannual deviations. In both cases, high negative correlations (–0.76 and

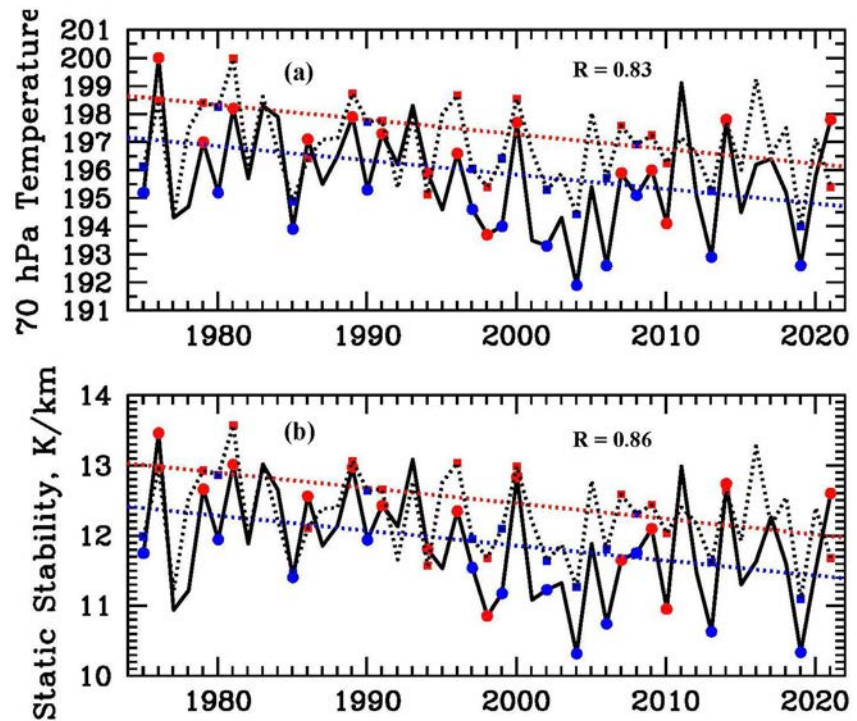


**Figure 10.** (a) Comparison of the 70 hPa mean tropical DJF temperature time series of Figure S3a in Supporting Information S1 (solid line) with an empirical model (dotted line) based on the observed sensitivity of interannual temperature deviations to early winter eddy heat flux anomalies. (b) Same format as (a) but for the 70 to 100 hPa mean tropical DJF static stability time series of Figure 7b.

−0.80) and significant regression slopes are obtained. As shown in Figure 9a, the mean sensitivity of interannual 70 hPa temperature reductions in DJF to interannual early winter eddy heat flux anomalies is  $-0.77 \pm 0.15$  K per 100 K-m/s. This value is  $\sim 30\%$  less than was estimated from the 2003–2004 winter alone and is more representative of the mean sensitivity for most years. As shown in Figure 9b, the mean sensitivity of tropical 70 to 100 hPa interannual static stability deviations to early winter eddy heat flux anomaly interannual deviations is  $-0.32 \pm 0.05$  K/km per 100 K-m/sec.

Figure 10 shows the result of applying the interannual sensitivities of Figure 9 together with the observational early winter eddy heat flux anomalies of Figure 8a to calculate model time series of mean tropical DJF 70 hPa temperatures and 70 to 100 hPa static stabilities (irregular dashed lines). Also shown are the observational temperature and static stability time series for comparison (solid lines). Blue and red symbols again identify strong QBOE and QBOW years, respectively. High correlation coefficients of 0.83 and 0.86 are obtained. Regression fits to the model QBOW years (linear red dashed lines) and the model QBOE years (linear blue dashed lines) are shown in both parts of the figure. These regression lines have slopes ( $\sim -0.5$  K/decade and  $\sim -0.3$  K/km per decade) that are comparable to those of the corresponding observational regression lines of Figures S3a in Supporting Information S1; Figure 7b.

## 6. Possible Relation to Increases in SSW Occurrence Rate and Arctic Sea Ice Loss

A question raised by this analysis is the origin of the positive trends in early winter wave forcing and the flat or negative trends in late-winter wave forcing shown in Figure 8. Consistent with the positive early winter trends, several studies have previously found evidence for statistically significant upward trends since 1980 in the frequency of weak stratospheric polar vortex states in the fall and winter seasons (Cohen et al., 2021; Kretschmer, Coumou et al., 2018). Another recent study has found evidence for a statistically significant increase in the occurrence rate and strengths of SSWs from the 1980s to the 2010s (Li et al., 2023). While the latter authors emphasized that identification of possible causes of the observed increase in SSW frequency and strength requires further study, they speculated that it could be “related to changes in polar-vortex dynamics over the recent decades ... partly

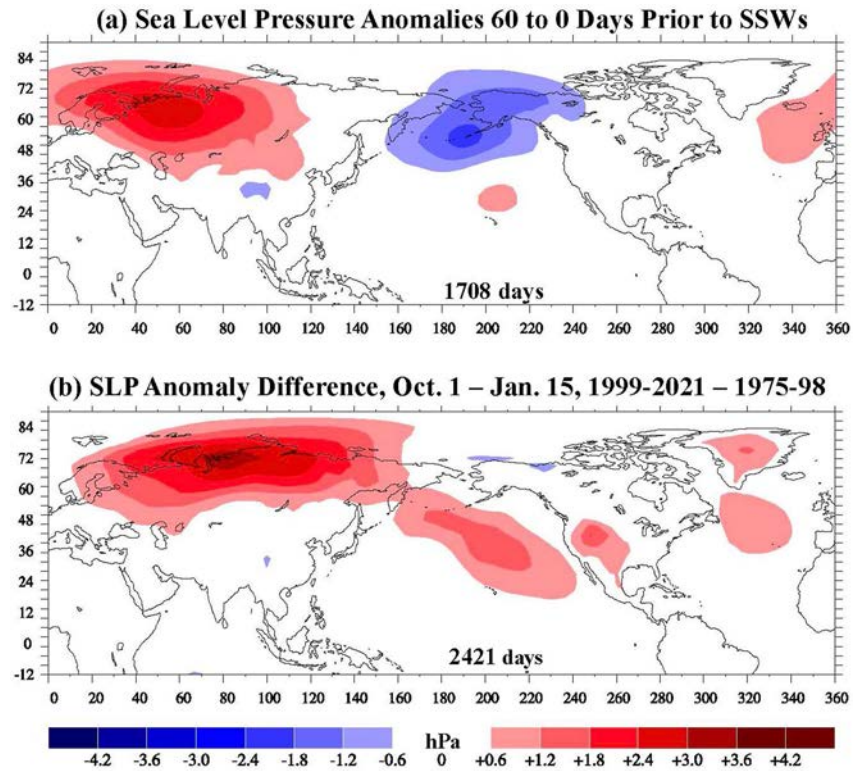


**Figure 11.** (a) Sea level pressure anomaly composites for up to 60 days prior to 28 SSWs occurring during 1974–2021; (b) differences between sea level pressure (SLP) anomaly composites during early winter (October 1–January 15) for the second part of the 1975 to 2021 period minus the first part.

induced by anthropogenic climate change in the polar regions (e.g., Kretschmer, Cohen, et al., 2018; Kretschmer, Coumou et al., 2018).”

As discussed by Kretschmer, Coumou et al. (2018) and Kretschmer, Cohen, et al. (2018), previous work (see the review by Cohen et al., 2014; their Figure B2) suggests that Arctic sea ice loss peaking at the time of the seasonal minimum in September combined with increased autumn snow cover over northern Eurasia can increase planetary wave amplitudes in the lower troposphere in early winter. The Eurasian snow cover component appears to be needed because a polar heating anomaly alone, due solely to the ice loss, would be expected to produce only a weak Rossby wave response under most conditions (Woollings et al., 2023). If enhanced wave amplitudes are produced, they would propagate into the stratosphere and break, weakening the stratospheric polar vortex, and increasing the probability of SSWs. Arctic sea ice concentrations near the time of the September minimum have declined throughout the period since satellite observations began in 1979, accelerating somewhat after 2000 (e.g., <https://climate.nasa.gov/vital-signs/arctic-sea-ice/>). Hence, this represents a possible hypothesis for explaining the observed increase in early winter wave forcing (Figure 8a) as well as the increasing frequency and strength of SSWs (Li et al., 2023).

Previous work has also found that SSWs tend to be preceded by distinct sea level pressure anomalies (e.g., Kretschmer, Coumou et al., 2018, and references therein). For comparison to these prior results, Figure 11a shows sea level pressure anomaly composites for the 60 days prior to the central dates of 28 SSWs occurring during 1974–2021. Of these 28 SSWs, 26 occurred during 1979–2019 and are listed in Table 2 of HTG23. The remaining two occurred on 9 January 1977, and 5 January 2021 (see Section 2 for references). All grid points within the colored areas are significant at the 95% confidence level according to a two-sided Student's *t* test, accounting for autocorrelation. The largest positive and negative anomalies occur over northwestern Eurasia and the northernmost Pacific, respectively. These anomalies constructively interfere with the climatological sea level pattern characterized by the Siberian high and the Aleutian low, thereby increasing tropospheric quasi-stationary wave amplitudes. The corresponding 100 hPa meridional eddy heat flux anomalies are characterized by strong

enhancements over northern Eurasia and the northernmost Pacific (see, e.g., Figure 8d of Kretschmer, Coumou et al., 2018). In this regard, it is of interest that the analysis of Li et al. (2023) determined the geographic onset location of the 43 SSWs that they identified, defined as the location on the onset date where the maximum temperature anomaly occurred within a specified threshold exceedance area in the stratosphere. They found that about 75% of the onset locations occurred over northern Eurasia and the adjacent polar ocean region (see their Figure 10d).

Following an SSW, the reversal of the polar vortex produces descent and warming of air at high latitudes in subsequent weeks, shifting jet streams and helping to produce a negative phase of the North Atlantic Oscillation (see the review by Baldwin et al., 2021). The post-SSW sea level pattern is characterized by high pressure over the Arctic and low pressure anomalies at middle latitudes, peaking over the North Atlantic (see, e.g., Figure 4a of Butler et al., 2017).

Figure 11b shows the difference between a composite of early winter sea level pressure anomalies for the second part of the period considered here (1998–1999 to 2020–2021; 23 years) and a similar composite for the first part (1974–1975 to 1997–1998; 24 years). It is one measure of the change with time during the study period of the sea level pressure anomalies in late fall and early winter. In each year, mean anomalies were first calculated for the Oct. 1 to Jan. 15 seasonal period before the compositing was done. The total number of considered days in the 23-year second period is given in the figure. Because of the large number of composited years, all grid points within the colored areas are significant at the 95% confidence level.

The largest positive difference anomaly in Figure 11b is centered in northern Eurasia just south of the Barents and Kara seas where the largest area of Arctic sea ice declines in the fall season have occurred (e.g., Overland et al., 2021; their Figure 1). Previous work has found that high pressure over this region is associated with Barents and Kara sea ice loss in autumn and increased Eurasian snow cover in October (Cohen et al., 2014; Kim et al., 2014; Kretschmer et al., 2016). September Arctic sea ice extent has declined while October Eurasian snow cover extent has increased continuously since satellite observations began in 1979 (Cohen et al., 2021; their Figures S1 and S2). As discussed by the latter authors, the increased autumn Eurasian snow cover is driven partly by the sea ice loss, which increases available moisture in the Arctic. The positive difference anomaly in Figure 11b centered in northern Eurasia is in the same region where positive sea level pressure anomalies are observed in the months prior to SSWs (Figure 11a; see also Figure 8b of Kretschmer, Coumou et al., 2018). It is also in the same region where a majority of SSW onset locations were identified by Li et al. (2023), as noted above. During the ~10 days prior to SSWs, the meridional eddy heat flux at northern latitudes is strongly enhanced (e.g., Figure 8d of Kretschmer, Coumou et al., 2018). Such sea level pressure anomalies in the latter half of the record would therefore increase planetary wave amplitudes, favoring increased extratropical wave forcing and an increased frequency of SSWs in early winter.

Coupled climate model experiments would be useful for testing whether sea level pressure differences similar to those of Figure 11b are sufficient to produce a Rossby wave response that could explain the positive trends in extratropical wave forcing during early winter found in Figure 8a.

## 7. Summary and Discussion

As summarized in Section 3, in agreement with Klotzbach et al. (2019) and Sakaeda et al. (2020), while some evidence for a QBO-MJO connection in boreal winter is present as far back as the early 1960s (Figures 1a and 2c), a clear connection is mainly found since the early 1980s (Figure 2b). The apparent strengthening of the connection has occurred during a period of declining boreal winter static stability at near-equatorial latitudes in the lowermost stratosphere (70–100 hPa; Figure 1b) and uppermost troposphere (100–200 hPa; Figure S1a in Supporting Information S1).

A combination of several factors related to climate change could be responsible for the observed reductions of tropical static stability and associated strengthening of the QBO-MJO connection since the mid-1970s. As pointed out originally by Klotzbach et al. (2019), observed declines in tropical upper tropospheric (100–200 hPa) static stability (Figure S1a in Supporting Information S1) caused mainly by positive trends in 200 hPa temperature (Figure S5 in Supporting Information S1) would have helped to destabilize the altitude range where MJO convection typically extends, possibly enhancing the ability of the QBO to produce a modulation.

Simultaneous cooling of the tropical lower stratosphere is also occurring, with stratospheric ozone depletion being a contributor during 1979–1995 in addition to a steady contribution from greenhouse gas emissions (Aquila et al., 2016; Ramaswamy and Schwarzkopf, 2002). However, as found here, interannual variability of DJF mean MJO amplitudes correlates best with tropical lower stratospheric (70–100 hPa) static stability (Figure 2) which, in turn, correlates inversely ( $R = -0.87$ ; Figure 2b) with extratropical wave forcing in early winter since 1979 (Figure 3b). Long-term positive trends in early winter extratropical wave forcing since that time (Figure 8a) may therefore have contributed significantly to reducing tropical lower stratospheric static stabilities and strengthening the QBO-MJO connection during the post-satellite era.

The weakness of the relationship prior to 1979 could be due partly to reduced data quality and/or to anomalous occurrences of strong early winter wave forcing during QBOW years in 1959–1960, 1967–1968, and 1969–1970. The latter years coincided with unusual occurrences of early winter SSWs during QBOW. Reduced reanalysis data quality in the pre-satellite era before 1979 is also expected due to the sparsity of radiosonde stations in the tropics. Tropical 70 to 100 hPa static stabilities remained relatively high prior to 1979 except during four strong QBOE years (1960–1961, 1965–1966, 1968–1969, and 1972–1973), which were all characterized by moderate to high DJF mean MJO amplitudes (Figures 1a and 1b).

Because of the anomalous behavior and/or reduced data quality in the early part of the record, Sections 4 and 5 focused on the period after the mid-1970s. The purpose was to evaluate whether the apparent strengthening of the QBO-MJO connection after the early 1980s could be related to negative trends in tropical static stability and positive trends in early winter extratropical wave forcing since that time. Most of the decline in 70–100 hPa static stability since the mid-1970s and most of its interannual variability can be attributed to temperature variability at the 70 hPa level since 100 hPa temperatures in boreal winter have remained relatively constant (Figure S3 in Supporting Information S1). As shown in Section 4, the decline of 70 hPa equatorial temperature to its mid-winter minimum is, in at least some years, mainly attributable to increases in extratropical wave forcing in late fall and early winter, which accelerate the BDC and increase the tropical upwelling rate.

As found in Section 5 (Figure 10), a simplified model based on the observed early winter meridional eddy heat fluxes and empirically estimated sensitivities on interannual time scales yields model time series that correlate very well with the observed tropical 70 hPa temperature and 70 to 100 hPa static stability time series. The model time series have negative trends that are comparable to those estimated from the observed time series.

As reviewed in Section 6, the positive wave forcing trends in early winter derived here from ERA5 data are consistent with previous evidence for an increasing frequency of weak polar vortex states in the fall and winter seasons, increasing SSW occurrence rates, and increasing SSW main phase strengths from the 1980s to the 2010s (Cohen et al., 2021; Kretschmer, Cohen, et al., 2018; Kretschmer, Coumou et al., 2018; Li et al., 2023). As also reviewed there, previous work has shown that Arctic sea ice loss in autumn and the associated increase in snow cover over northern Eurasia can produce sea level pressure anomalies that increase planetary wave amplitudes in early winter (Cohen et al., 2014, 2021; Kretschmer, Coumou et al., 2018). When these enhanced waves propagate into the stratosphere and break, they increase the probability of occurrence of weak vortex states and SSWs. A distinct set of sea level pressure anomalies, including a positive anomaly over northern Eurasia, is a known precursor of weak polar vortex states and SSWs (Figure 11a; Kretschmer, Coumou et al., 2018, their Figure 8b). As found in Figure 11b, the positive sea level pressure anomaly over northern Eurasia has increased in strength during the second part of the study period relative to the first part. This increase in sea level pressure anomaly strength over northern Eurasia has coincided with a period since 1979 of declining autumn Arctic sea ice extent and increasing Eurasian snow cover, a time period referred to as the “Arctic Amplification” era. The observed negative trends in Arctic sea ice extent and positive trends in Eurasian snow cover are therefore a possible significant contributor to the observed positive trends since the mid-1970s in early winter wave forcing (Figure 8a), the increased frequency of weak polar vortex states (Cohen et al., 2021; Kretschmer, Coumou et al., 2018), and the increased occurrence rates of SSWs (Li et al., 2023).

Coupled climate model experiments are needed to test whether Arctic sea ice loss and the associated increased Eurasian snow cover in autumn are the main drivers of the observed long-term increases in early winter extratropical wave forcing since the mid-1970s. If positive results are obtained and if reductions of tropical lower stratospheric static stability since that time have in fact strengthened the QBO-MJO connection, then it would follow from the analysis of Section 5 that north polar climate change has been a significant contributor to the observed strengthening.

### Data Availability Statement

The ERA5 1959–2021 data used here (Bell et al., 2021; Hersbach et al., 2020) are available from the ECMWF. The equatorial zonal wind data used to determine the phase of the QBO (updated from Naujokat, 1986) are available from the Free University of Berlin at <https://www.geo.fu-berlin.de/met/ag/strat/produkte/qbo/qbo.dat>. The OMI (MJO amplitude) values starting in January 1979 are available from NOAA at <https://psl.noaa.gov/mjo/mjoindex/omi.lx.txt>. The OMI values for times prior to 1979 were calculated from ERA5 OLR model data using the Python code detailed in Hoffmann et al. (2021), available at <http://dx.doi.org/10.5281/zenodo.3613752>.

### Acknowledgments

Support from the NSF Climate and Large-Scale Dynamics program (2039384) and the NASA Living with a Star program (80NSSC21K1309) is appreciated. Important assistance was provided by Drs. Thomas J. Galarneau, Jr. and Natasha E. Trencham. We thank Dr. Hua Lu of the British Antarctic Survey for an early discussion and for suggesting investigation of Arctic sea ice loss as a possible factor in producing increases in early winter extratropical wave forcing. Thanks also to Dr. Xiaocen Shen of the University of Reading for bringing to our attention the work by Monnin et al. (2021) showing that surface impacts of SSWs may be larger in early winter due to the larger stratospheric polar vortex anomaly compared to climatology. Useful criticisms from three anonymous reviewers contributed substantially to improving the original manuscript.

### References

- Abhik, S., & Hendon, H. H. (2019). Influence of the QBO on the MJO during coupled model multiweek forecasts. *Geophysical Research Letters*, 46(15), 9213–9221. <https://doi.org/10.1029/2019GL083152>
- Abhik, S., Hendon, H. H., & Wheeler, M. C. (2019). On the sensitivity of convectively coupled equatorial waves to the quasi-biennial oscillation. *Journal of Climate*, 32(18), 5833–5847. <https://doi.org/10.1175/JCLI-D-19-0010.1.s1>
- Adames, A. F., & Kim, D. (2016). The MJO as a dispersive, convectively coupled moisture wave: Theory and observations. *Journal of the Atmospheric Sciences*, 73(3), 913–941. <https://doi.org/10.1175/JAS-D-15-0170.1>
- Andrews, D. G., Holton, J. R., & Leovy, C. B. (1987). *Middle atmosphere dynamics* (p. 489). Academic Press.
- Aquila, V., Swartz, S. H., Waugh, D. W., Colarco, P. R., Pawson, S., Polvani, L. M., & Stolarski, R. S. (2016). Isolating the roles of different forcing agents in global stratospheric temperature changes using model integrations with incrementally added single forcings. *Journal of Geophysical Research: Atmospheres*, 121(13), 8067–8082. <https://doi.org/10.1002/2015JD023841>
- Baldwin, M. P., Ayarzagüena, B., Birner, T., Butchart, N., Butler, A. H., Charlton-Perez, A. J., et al. (2021). Sudden stratospheric warmings. *Reviews of Geophysics*, 59(1), e2020RG000708. <https://doi.org/10.1029/2020RG000708>
- Baldwin, M. P., Gray, L. J., Dunkerton, T. J., Hamilton, K., Haynes, P. H., Randel, W. J., et al. (2001). The quasi-biennial oscillation. *Reviews of Geophysics*, 39(2), 179–229. <https://doi.org/10.1029/1999rg000073>
- Bell, B., Hersbach, H., Simmons, A., Berrisford, P., Dahlgren, P., Horányi, A., et al. (2021). The ERA5 global reanalysis: Preliminary extension to 1950. *Quarterly Journal of the Royal Meteorological Society*, 147(741), 4186–4227. <https://doi.org/10.1002/qj.4174>
- Butler, A. H., Sjöberg, J. P., Seidel, D. J., & Rosenlof, K. H. (2017). A sudden stratospheric warming compendium. *Earth System Science Data*, 9(1), 63–76. <https://doi.org/10.5194/essd-9-63-2017>
- Charlton, A. J., & Polvani, L. M. (2007). A new look at stratospheric sudden warmings. Part I: Climatology and modeling benchmarks. *Journal of Climate*, 20(3), 449–469. <https://doi.org/10.1175/JCLI3996.1>
- Charney, J. G., & Drazin, P. G. (1961). Propagation of planetary-scale disturbances from the lower into the upper atmosphere. *Journal of Geophysical Research*, 66(1), 83–109. <https://doi.org/10.1029/JZ066i001p00083>
- Cohen, J., Agel, L., Barlow, M., Garfinkel, C. I., & White, I. (2021). Linking Arctic variability and change with extreme winter weather in the United States. *Science*, 373(6559), 1116–1121. <https://doi.org/10.1126/science.abi9167>
- Cohen, J., Screen, J. A., Furtado, J. C., Barlow, M., Whittleston, D., Cournou, D., et al. (2014). Recent Arctic amplification and extreme mid-latitude weather. *Nature Geoscience*, 7(9), 627–637. <https://doi.org/10.1038/NGEO2234>
- Davis, N. A., Richter, J. H., Glanville, A. A., Edwards, J., & LaJoie, E. (2022). Limited surface impacts of the January 2021 sudden stratospheric warming. *Nature Communications*, 13(1), 1136. <https://doi.org/10.1038/s41467-022-28836-1>
- Domeisen, D., Butler, A. H., Charlton-Perez, A. J., Ayarzagüena, B., Baldwin, M. P., Dunn-Sigouin, E., et al. (2019). The role of the stratosphere in subseasonal to seasonal prediction: 2. Predictability arising from stratosphere-troposphere coupling. *Journal of Geophysical Research: Atmospheres*, 125. <https://doi.org/10.1029/2019JD030923>
- Elsbury, D., Peings, Y., & Magnusdottir, G. (2021). CMIP6 models underestimate the Holton-Tan effect. *Geophysical Research Letters*, 48(24), e2021GL094083. <https://doi.org/10.1029/2021GL094083>
- Fueglistaler, S., Abalos, M., Flannaghan, T. J., Lin, P., & Randel, W. J. (2014). Variability and trends in dynamical forcing of tropical lower stratospheric temperatures. *Atmospheric Chemistry and Physics*, 14(24), 13439–13453. <https://doi.org/10.5194/acp-14-13439-2014>
- Garfinkel, C. I., Benedict, J. J., & Maloney, E. D. (2014). Impact of the MJO on the boreal winter extratropical circulation. *Geophysical Research Letters*, 41(16), 6055–6062. <https://doi.org/10.1002/2014GL061094>
- Garfinkel, C. I., Feldstein, S. B., Waugh, D. W., Yoo, C., & Lee, S. (2012). Observed connection between sudden stratospheric warmings and the Madden-Julian oscillation. *Geophysical Research Letters*, 39(18), L18807. <https://doi.org/10.1029/2012GL053144>
- Gray, L. J., Brown, M. J., Knight, J., Andrews, M., Lu, H., O'Reilly, C., & Anstey, J. (2020). Forecasting extreme stratospheric polar vortex events. *Nature Communications*, 11(1), 4630. <https://doi.org/10.1038/s41467-020-18299-7>
- Gray, L. J., Crooks, S., Pascoe, C., Sparrow, S., & Palmer, M. (2004). Solar and QBO influences on the timing of stratospheric sudden warmings. *Journal of the Atmospheric Sciences*, 61(23), 2777–2796. <https://doi.org/10.1175/JAS-3297.1>
- Hartmann, D. L., Holton, J. R., & Fu, Q. (2001). The heat balance of the tropical tropopause, cirrus, and stratospheric dehydration. *Geophysical Research Letters*, 28(10), 1969–1972. <https://doi.org/10.1002/2000GL012833>
- Haynes, P., Hitchcock, P., Hitchman, M., Yoden, S., Hendon, H., Kiladis, G., et al. (2021). The influence of the stratosphere on the tropical troposphere. *Journal of the Meteorological Society of Japan*, 99(4), 803–845. <https://doi.org/10.2151/jmsj.2021-040>
- Hendon, H. H., & Abhik, S. (2018). Differences in vertical structure of the Madden-Julian Oscillation associated with the quasi-biennial oscillation. *Geophysical Research Letters*, 45(9), 4419–4428. <https://doi.org/10.1029/2018GL077207>
- Hersbach, H., Bell, B., Berrisford, P., Hirahara, S., Horányi, A., Muñoz Sabater, J., et al. (2020). The ERA5 global reanalysis. *Quarterly Journal of the Royal Meteorological Society*, 146(730), 1999–2049. <https://doi.org/10.1002/qj.3803>
- Hoffmann, C. G., Kiladis, G. N., Gehne, M., & von Savigny, C. (2021). A Python package to calculate the OLR-based index of the Madden-Julian oscillation (OMI) in climate science and weather forecasting. *Journal of Open Research Software*, 9(1), 9. <https://doi.org/10.5334/jors.331>
- Hoffmann, C. G., & von Savigny, C. (2019). Indications for a potential synchronization between the phase evolution of the Madden-Julian oscillation and the solar 27-day cycle. *Atmospheric Chemistry and Physics*, 19(7), 4235–4256. <https://doi.org/10.5194/acp-19-4235-2019>
- Holton, J. R., & Tan, H. C. (1980). The influence of the equatorial quasi-biennial oscillation on the global circulation at 50 mb. *Journal of the Atmospheric Sciences*, 37(10), 2200–2208. [https://doi.org/10.1175/1520-0469\(1980\)037<2200:TIOTEQ>2.0.CO;2](https://doi.org/10.1175/1520-0469(1980)037<2200:TIOTEQ>2.0.CO;2)
- Hood, L. L. (2017). QBO/solar modulation of the boreal winter Madden-Julian oscillation: A prediction for the coming solar minimum. *Geophysical Research Letters*, 44(8), 3849–3857. <https://doi.org/10.1002/2017GL072832>

- Hood, L. L. (2018). Short-term solar modulation of the Madden-Julian climate oscillation. *Journal of the Atmospheric Sciences*, 75(3), 857–873. <https://doi.org/10.1175/JAS-D-17-0265.1>
- Hood, L. L., Redman, M., Johnson, W., & Galarneau, T. J., Jr. (2020). Stratospheric influences on the MJO-induced Rossby wave train: Effects on intraseasonal climate. *Journal of Climate*, 33(1), 365–389. <https://doi.org/10.1175/JCLI-D-18-0811.1>
- Hood, L. L., & Soukharev, B. E. (2003). Quasi-decadal variability of the tropical lower stratosphere: The role of extratropical wave forcing. *Journal of the Atmospheric Sciences*, 60(19), 2389–2403. [https://doi.org/10.1175/1520-0469\(2003\)060<2389:QVOTTL>2.0.CO;2](https://doi.org/10.1175/1520-0469(2003)060<2389:QVOTTL>2.0.CO;2)
- Hood, L. L., Trencham, N. E., & Galarneau, T. J., Jr. (2023). QBO/solar influences on the tropical Madden-Julian oscillation: A mechanism based on extratropical wave forcing in late fall and early winter. *Journal of Geophysical Research: Atmospheres*, 128(6), e2022JD037824. <https://doi.org/10.1029/2022JD037824>
- Hood, L. L., Trencham, N. E., Hoopes, C. A., & Galarneau, T. J., Jr. (2023). Lagged strengthening of the Madden-Julian oscillation following early winter sudden stratospheric warmings: Implications for the origin of the QBO/solar-MJO connection. In *Paper presented at IUGG Berlin 2023, Berlin, Germany, July 12, 2023, session M01a, abstract 1985*. Retrieved from <https://www.iugg2023berlin.org>
- Jiang, X., Adames, A. F., Kim, D., Maloney, E. D., Lin, H., Kim, H., et al. (2020). Fifty years of research on the Madden-Julian oscillation: Recent progress, challenges, and perspectives. *Journal of Geophysical Research: Atmospheres*, 125(17), e2019JD030911. <https://doi.org/10.1029/2019JD030911>
- Karpechko, A. Y. (2018). Predictability of sudden stratospheric warmings in the ECMWF extended-range forecast system. *Monthly Weather Review*, 146(4), 1063–1075. <https://doi.org/10.1175/MWR-D-17-0317.1>
- Kiehl, J. T., & Solomon, S. (1986). On the radiative balance of the stratosphere. *Journal of the Atmospheric Sciences*, 43(14), 1525–1534. [https://doi.org/10.1175/1520-0469\(1986\)043<1525:OTRBOT>2.0.CO;2](https://doi.org/10.1175/1520-0469(1986)043<1525:OTRBOT>2.0.CO;2)
- Kiladis, G. N., Dias, J., Straub, K. H., Wheeler, M. C., Tulich, S. N., Kikuchi, K., et al. (2014). A comparison of OLR and circulation-based indices for tracking the MJO. *Monthly Weather Review*, 142(5), 1697–1715. <https://doi.org/10.1175/MWR-D-13-00301.1>
- Kim, B.-M., Son, S.-W., Min, S.-K., Jeong, J.-H., Kim, S.-J., Zhang, X., et al. (2014). Weakening of the stratospheric polar vortex by Arctic sea-ice loss. *Nature Communications*, 5(1), 4646. <https://doi.org/10.1038/ncomms5646>
- Kim, H., Caron, J. M., Richter, J. H., & Simpson, I. R. (2020). The lack of QBO-MJO connection in CMIP6 models. *Geophysical Research Letters*, 47(11), e2020GL087295. <https://doi.org/10.1029/2020GL087295>
- Klotzbach, P., Abhik, S., Hendon, H., Bell, M., Lucas, C., Marshall, A. G., & Oliver, E. C. J. (2019). On the emerging relationship between the stratospheric quasi-biennial oscillation and the Madden-Julian oscillation. *Scientific Reports*, 9(1), 2981. <https://doi.org/10.1038/s41598-019-40034-6>
- Kodera, K., Nasuno, T., Son, S.-W., Eguchi, N., & Harada, Y. (2023). Influence of the stratospheric QBO on seasonal migration of the convective center across the Maritime Continent. *Journal of the Meteorological Society of Japan*, 101(6), 445–459. Early Online Release. <https://doi.org/10.2151/jmsj.2024-001>
- Kretschmer, M., Cohen, J., Matthias, V., Runge, J., & Coumou, D. (2018). The different stratospheric influence on cold-extremes in Eurasia and North America. *Climate and Atmospheric Science*, 1, 44. <https://doi.org/10.1038/s41612-018-0054-4>
- Kretschmer, M., Coumou, D., Agel, L., Barlow, M., Tziperman, E., & Cohen, J. (2018). More persistent weak stratospheric polar vortex states linked to cold extremes. *Bulletin of the American Meteorological Society*, 99(1), 49–60. <https://doi.org/10.1175/BAMS-D-16-0259.1>
- Kretschmer, M., Coumou, D., Donges, J. F., & Runge, J. (2016). Using causal effect networks to analyze different Arctic drivers of midlatitude winter circulation. *Journal of Climate*, 29(11), 4069–4081. <https://doi.org/10.1175/JCLI-D-15-0654.1>
- Li, Y., Kirchengast, G., Schwaerz, M., & Yuan, Y. (2023). Monitoring sudden stratospheric warmings under climate change since 1980 based on reanalysis data verified by radio occultation. *Atmospheric Chemistry and Physics*, 23(2), 1259–1284. <https://doi.org/10.5194/acp-23-1259-2023>
- Lim, Y., & Son, S.-W. (2020). QBO-MJO Connection in CMIP5 models. *Journal of Geophysical Research: Atmospheres*, 125(12), e2019JD032157. <https://doi.org/10.1029/2019JD032157>
- Lim, Y., & Son, S.-W. (2022). QBO wind influence on MJO-induced temperature anomalies in the upper troposphere and lower stratosphere in an idealized model. *Journal of the Atmospheric Sciences*, 79(9), 2219–2228. <https://doi.org/10.1175/JAS-D-21-0296.1>
- Lim, Y., Son, S.-W., Marshall, A. G., Hendon, H. H., & Seo, K.-H. (2019). Influence of the QBO on MJO prediction skill in the subseasonal-to-seasonal prediction models. *Climate Dynamics*, 53(3–4), 1681–1695. <https://doi.org/10.1007/s00382-019-04719-y>
- Lu, H., Hitchman, M. H., Gray, L. J., Anstey, J. A., & Osprey, S. M. (2020). On the role of Rossby wave breaking in the quasi-biennial modulation of the stratospheric polar vortex during boreal winter. *Quarterly Journal of the Royal Meteorological Society*, 146(729), 1939–1959. <https://doi.org/10.1002/qj.3775>
- Madden, R. A., & Julian, P. R. (1994). Observations of the 40–50-day tropical oscillation—A review. *Monthly Weather Review*, 122(5), 814–837. [https://doi.org/10.1175/1520-0493\(1994\)122<0814:OOTDTP>2.0.CO;2](https://doi.org/10.1175/1520-0493(1994)122<0814:OOTDTP>2.0.CO;2)
- Maloney, E. D., Adames, A. F., & Bui, H. X. (2019). Madden-Julian oscillation changes under anthropogenic warming. *Nature Climate Change*, 9(1), 26–33. <https://doi.org/10.1038/s41558-018-0331-6>
- Martin, Z., Orbe, C., Wang, S., & Sobel, A. H. (2021). The MJO-QBO relationship in a GCM with stratospheric nudging. *Journal of Climate*, 34, 4603–4624. <https://doi.org/10.1175/JCLI-D-20-0636.1>
- Martin, Z., Son, S.-W., Butler, A., Hendon, H., Kim, H., Sobel, A., et al. (2021). The influence of the quasi-biennial oscillation on the Madden-Julian oscillation. *Nature Reviews Earth & Environment*, 2(7), 477–489. <https://doi.org/10.1038/s43017-021-00173-9>
- Mlynczak, M. G., Mertens, C. J., Garcia, R. R., & Portmann, R. W. (1999). A detailed evaluation of the stratospheric heat budget. 2. Global radiation balance and diabatic circulations. *Journal of Geophysical Research*, 104(D6), 6039–6066. <https://doi.org/10.1029/1998JD200099>
- Monnin, E., Kretschmer, M., & Polichtchouk, I. (2021). The role of the timing of sudden stratospheric warmings for precipitation and temperature anomalies in Europe. *International Journal of Climatology*, 42(6), 3448–3462. <https://doi.org/10.1002/joc.7426>
- Naujokat, B. (1986). An update of the observed quasi-biennial oscillation of the stratospheric winds over the tropics. *Journal of the Atmospheric Sciences*, 43(17), 1873–1877. [https://doi.org/10.1175/1520-0469\(1986\)043<1873:AUTOOQ>2.0.CO;2](https://doi.org/10.1175/1520-0469(1986)043<1873:AUTOOQ>2.0.CO;2)
- Newman, P. A., & Rosenfield, J. E. (1997). Stratospheric thermal damping times. *Geophysical Research Letters*, 24(4), 433–436. <https://doi.org/10.1029/96GL03720>
- Nishimoto, E., & Yoden, S. (2017). Influence of the stratospheric quasi-biennial oscillation on the Madden-Julian oscillation during austral summer. *Journal of the Atmospheric Sciences*, 74(4), 1105–1125. <https://doi.org/10.1175/JAS-D-16-0205.1>
- Noguchi, S., Kuroda, Y., Kodera, K., & Watanabe, S. (2020). Robust enhancement of tropical convective activity by the 2019 Antarctic sudden stratospheric warming. *Geophysical Research Letters*, 47(15), e2020GL088743. <https://doi.org/10.1029/2020GL088743>
- Overland, J. E., Ballinger, T. J., Cohen, J., Francis, J. A., Hanna, R., Jaiser, R., et al. (2021). How do intermittency and simultaneous processes obfuscate the Arctic influence on midlatitude winter extreme weather events? *Environmental Research Letters*, 16(4), 043002. <https://doi.org/10.1088/1748-9326/abdb5d>

- Ramaswamy, V., & Schwarzkopf, M. D. (2002). Effects of ozone and well-mixed gases on annual mean stratospheric temperature trends. *Geophysical Research Letters*, *29*(22), 21-1–21-4. <https://doi.org/10.1029/2002GL015141>
- Randel, W. J., Garcia, R. R., & Wu, F. (2002). Time-dependent upwelling in the tropical lower stratosphere estimated from the zonal-mean momentum budget. *Journal of the Atmospheric Sciences*, *59*(13), 2141–2152. [https://doi.org/10.1175/1520-0469\(2002\)059<2141:TDUITT>2.0.CO;2](https://doi.org/10.1175/1520-0469(2002)059<2141:TDUITT>2.0.CO;2)
- Rao, J., Garfinkel, C. I., Chen, H., & White, I. P. (2019). The 2019 New Year stratospheric sudden warming and its real-time predictions in multiple S2S models. *Journal of Geophysical Research: Atmospheres*, *124*(21), 11155–11174. <https://doi.org/10.1029/2019JD030826>
- Roundy, P. E. (2022). Quasi-biennial oscillation impacts on Madden-Julian oscillation-associated tropical-extratropical interactions and Kelvin waves. *Quarterly Journal of the Royal Meteorological Society*, *148*(743), 907–919. <https://doi.org/10.1002/qj.4238>
- Sakaeda, N., Dias, J., & Kiladis, G. N. (2020). The unique characteristics and potential mechanisms of the MJO-QBO relationship. *Journal of Geophysical Research: Atmospheres*, *125*(17), e2020JD033196. <https://doi.org/10.1029/2020JD033196>
- Son, S. W. (2023). QBO-MJO connection: Two possible mechanisms. In *Paper presented at QBO workshop, Oxford University, Oxford, U.K., 27–31 March, 2023*. Retrieved from <https://sites.google.com/view/qbo-workshop-march-2023>
- Son, S.-W., Lim, Y., Yoo, C., Hendon, H., & Kim, J. (2017). Stratospheric control of the Madden-Julian oscillation. *Journal of Climate*, *30*(6), 1909–1922. <https://doi.org/10.1175/JCLI-D-16-0620.1>
- Toms, B. A., Barnes, E. A., Maloney, E. D., & van den Heever, S. C. (2020). The global teleconnection signature of the Madden-Julian oscillation and its modulation by the quasi-biennial oscillation. *Journal of Geophysical Research: Atmospheres*, *125*(7), e2020JD032653. <https://doi.org/10.1029/2020JD032653>
- Wang, J., Kim, H.-M., Chang, E. K. M., & Son, S.-W. (2018). Modulation of the MJO and North Pacific storm track relationship by the QBO. *Journal of Geophysical Research: Atmospheres*, *123*(8), 3976–3992. <https://doi.org/10.1029/2017JD027977>
- Woollings, T., Li, C., Drouard, M., Dunn-Sigouin, E., Elmetekawy, K. A., Hell, M., et al. (2023). The role of Rossby waves in polar weather and climate. *Weather and Climate Dynamics*, *4*(1), 61–80. <https://doi.org/10.5194/wed-4-61-2023>
- Yoo, C., & Son, S. W. (2016). Modulation of the boreal wintertime Madden-Julian oscillation by the stratospheric quasi-biennial oscillation. *Geophysical Research Letters*, *43*(3), 1392–1398. <https://doi.org/10.1002/2016GL067762>
- Zhang, C. (2013). Madden-Julian oscillation: Bridging weather and climate. *Bulletin of the American Meteorological Society*, *94*(12), 1849–1870. <https://doi.org/10.1175/BAMS-D-12-00026.1>
- Zhou, W., Yang, D., Xie, S.-P., & Ma, J. (2020). Amplified Madden-Julian oscillation impacts in the Pacific-North America region. *Nature Climate Change*, *10*(7), 654–660. <https://doi.org/10.1038/s41558-020-0814-0>